

Boundary and Relation Distillation for Semantic Segmentation

Dong Zhang¹, Pingcheng Dong¹, Xinting Hu², Long Chen³, Kwang-Ting Cheng¹

1. The Department of Electronic and Computer Engineering at HKUST.

2. Max Planck Institute for Informatics. 3. The Department of Computer Science and Engineering at HKUST.

Abstract

Recently, it has been revealed that small semantic segmentation (SS) models exhibit a tendency to make errors in maintaining boundary region completeness and preserving target region connectivity, despite their effective segmentation of the main object regions. To address these errors, we propose a targeted boundary and relation distillation (BRD) strategy using knowledge distillation from large teacher models to small student models. Specifically, the boundary distillation extracts explicit object boundaries from the hierarchical feature maps of the backbone network, subsequently enhancing the student model’s mask quality in boundary regions. Concurrently, the relation distillation transfers implicit relations from the teacher model to the student model using pixel-level self-relation as a bridge, ensuring that the student’s mask has strong target region connectivity. The proposed BRD is designed concretely for SS and is characterized by simplicity and efficiency. Through experimental evaluations on multiple SS datasets, including Pascal VOC 2012, Cityscapes, ADE20K, and COCO-Stuff 10K, we demonstrated that BRD significantly surpasses the current methods without increasing the inference costs, generating crisp region boundaries and smooth connecting regions that are challenging for small models.

1. Introduction

Semantic segmentation (SS) is a fundamental yet challenging research task in the community of computer vision, aiming at assigning a semantic label to each pixel in an input image [48, 79, 86]. However, deploying large and accurate SS models on resource-limited edge computing devices, e.g., mobile phones [91] and AI accelerators [85], poses significant challenges due to the high computational costs and large memory requirements [41, 78]. To overcome this challenge, knowledge distillation (KD) [30, 32, 76], a popular model compression technology, has been widely used to obtain satisfactory results with a small SS model (i.e., the student model) by emulating the behavior of a large SS model (i.e., the teacher model) [45, 68].

Despite the promising progress has been made by current KD methods on SS [17, 25, 45, 68, 74, 87], these methods primarily rely on coarse general knowledge (e.g., features and logits) and neglect the specific feature understanding over the object boundary and connecting regions [62, 87]. Particularly, since small student models can often segment the main object regions fairly well but fail in boundary and connecting regions [6, 24, 82], the conventional utilization of coarse general KD may not be effective enough and can be considered purposeless and redundant [25, 74, 88, 92], remaining a performance gap between the obtained results and the expected results [17, 63, 75]. As illustrated in Figure 1, the small student model (PSPNet-18 [93]) in (c) produces inferior results compared to the large teacher model (PSPNet-101 [93]) results in (b). The small model wrongly segments the boundary regions of “curtain” and “door” as the background category or other foreground objects, and produces fragmented “bed valance” and “chair”, breaking the regional relation connectivity. In general, the errors that occur in the results of small models can be summarized as *maintaining boundary region completeness* and *preserving target region connectivity*.

To address these problems and bridge the performance gap in SS, we propose a simple and clean KD strategy: boundary and relation distillation (BRD). BRD consists of *boundary distillation* and *relation distillation*, which are designed to address the common errors faced by small student models in maintaining boundary region completeness and preserving target region connectivity, respectively. Specifically, the *boundary distillation* synthesizes explicit object boundaries from the hierarchical backbone feature maps (ref. Sec. 4.2), thereby enhancing the completeness of the student’s masks in the boundary regions. At the same time, the *relation distillation* transfers implicit relation information from the teacher model to the student model using pixel-level self-relation as a bridge (ref. Sec. 4.3), ensuring that the student’s masks have strong target region connectivity. BRD is concretely designed for SS tasks. Compared to the commonly used feature-based and logit-based KD, our proposed BRD features more targeted distillation content and a more tailored distillation manner.

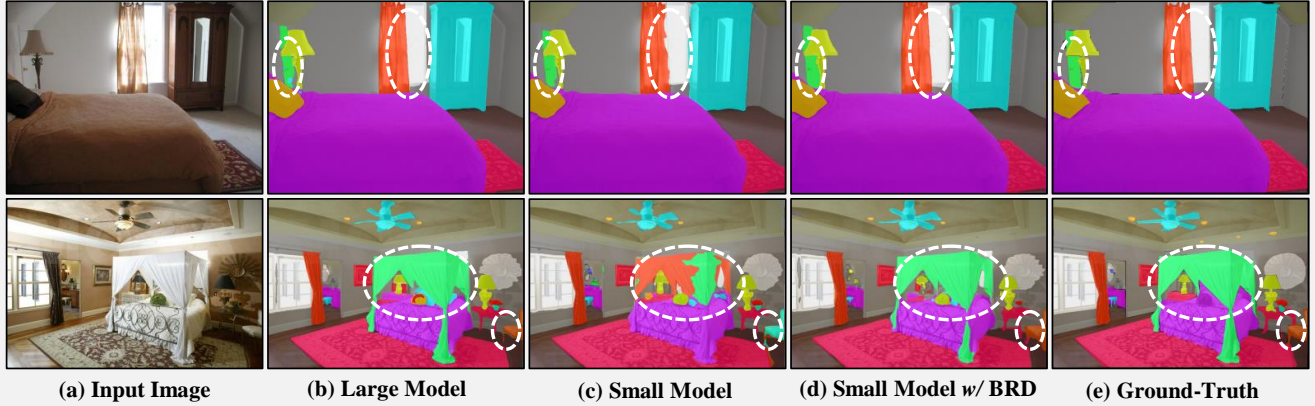


Figure 1. Two representative scenarios that small models are prone to segmentation errors [93]. Result comparisons between large models (b) and small models (c) show that the latter tend to make errors in maintaining boundary region completeness (e.g., the “curtain” and the “door”) and preserving foreground/background region connectivity (e.g., the “bed valance” and the “chair”), while both large and small models are capable of segmenting the main region of the object with satisfactory accuracy. With the help of our BRD in (d), small models can address the two types of errors, leading to crisp region boundaries and smooth connecting regions. “w/” denotes with the corresponding implementation. The white dashed lines highlight the areas where our method achieves better results. Samples are from the ADE20K dataset [100]. More visualization results will be given in the supplementary.

To demonstrate the superior performance of our BRD, we conducted extensive experiments on several challenging SS datasets, *i.e.*, Pascal VOC 2012 [21], Cityscapes [16], ADE20K [100], and COCO-Stuff 10K [5]. Qualitatively, BRD can generate crisp region boundaries and smooth connecting regions that were previously challenging for small SS models. Quantitatively, BRD consistently boosts baseline models’ accuracy, ultimately achieving very competitive accuracy without increasing the inference costs.

The main contributions are the following three-fold:

- It is observed that small SS models are prone to segmentation errors in maintaining boundary region completeness and preserving target region connectivity;
- We proposed a targeted KD strategy for SS, *boundary distillation* and *relation distillation*, to address the representative errors faced by small models;
- Experimental results on various baselines and datasets demonstrate the superior performance of our BRD over existing methods, achieving very competitive results.

2. Related Work

Semantic Segmentation (SS). SS aims at assigning each pixel in an input image to a specific category label (e.g., “desk”, “pedestrian”, and “car”), enabling a pixel-level semantic recognition of the given image [48, 79, 86, 87, 89]. The current SS architectures can be roughly classified into the following three categories based on their basic components: methods based on CNNs [33, 48, 51, 64, 79, 89], methods based on Transformers [46, 57, 69, 72, 96], and methods that combine CNNs and Transformers [20, 27, 38, 54, 70]. The key difference between these three types of architectures is the approach used for feature extraction and

how the extracted feature maps are utilized (e.g., enhancing the ability of CNNs-based models to capture contextual features [6, 9], increasing the ability of Transformer-based models to capture local features [54, 70], and leveraging low-level features to improve prediction performance [66, 72]) to achieve effective and efficient results. Concretely, due to inherent differences in feature extraction between CNNs and Transformer frameworks, these two methods exhibit slight performance differences [38, 54, 69, 96]. For example, CNNs-based methods are better at segmenting local object regions, while Transformer-based methods, due to their stronger contextual information, can produce more complete segmentation masks. Fortunately, the hybridization of CNNs and Transformers (e.g., CMT [27], CvT [70], and ConFormer [54]) leverage the strengths of both patterns, resulting in highly satisfactory segmentation results [29, 49, 66]. In addition to these fundamental categories, there are advanced methods that utilize task-specific tricks (e.g., graph reasoning [88], efficient attention [36], multi-scale transformer [22]) to improve the accuracy and efficiency of the performance. However, while current methods have achieved promising accuracy, deploying these models on resource-constrained edge computing devices (e.g., mobile phones [91] and AI accelerators [85]) remains challenging because these devices typically have limited computation resources and memory space [18, 19]. In this work, we do not intend to modify the network architecture. We investigate the result disparities between small and large models and propose a knowledge distillation strategy tailored to SS tasks. We aim at improving the segmentation accuracy of small models without requiring any additional training data or increasing the inference costs.

Knowledge Distillation (KD) in Computer Vision. KD aims at transferring the valuable knowledge from a large teacher model to a small student model, with the goal of improving the student model’s accuracy in inference [25, 26, 32, 45, 68]. The key factors for the success of KD are: 1) the types of knowledge being distilled (*e.g.*, features and logits), 2) the distillation strategies employed (*e.g.*, offline distillation [61], online distillation [28], and self-distillation [90]), and 3) the architecture of the teacher-student (*e.g.*, multi-teacher KD [80], attention-based KD [52], and graph-based KD [37]). While the effectiveness of existing KD methods has been validated, current methods mostly rely on the coarse general knowledge and do not consider the task-specific feature requirements [8, 25, 49, 59, 65]. Especially for SS tasks, models are highly sensitive to feature representations [48, 89, 96]. Therefore, coarse general KD may not be effective enough and can be considered purposeless and redundant [25, 74, 88, 92], remaining a performance gap between the obtained results and the expected results [17, 63, 75]. Recent studies have shown that task-specific patterns of KD can help further improve the performance of student models [98]. For example, in object detection, more specific localization KD leads to more accurate predictions than the coarse general knowledge [59, 99]. In this work, we also adopt the idea of task-specific KD for SS. Our contribution lies in proposing two KD schemes, namely *boundary distillation* and *relation distillation*, which target the weaknesses of small SS models, namely their tendency to make errors in maintaining boundary region completeness and preserving target region connectivity.

3. Preliminaries

During the training phase, KD intends to facilitate knowledge transfer from a large teacher model \mathbb{T} to a compact student model \mathbb{S} , with the primary goal of enhancing the accuracy of \mathbb{S} [25, 32, 35, 87, 90]. Typically, features and logits serve as a medium for knowledge propagation. In inference, only \mathbb{S} is required, and hence there is no increase in the computational costs. Generally, the temperature scaling strategy is employed to smooth the features/logits, thereby reducing prediction confidence and mitigating the problem of excessive self-assurance in \mathbb{T} [55]. KD can be expressed by minimizing the cross-entropy loss as follows:

$$\mathcal{L}_{KD} = -\tau^2 \sum_{i \in M} \sigma(\mathbf{T}_i)^{1/\tau} \log \left(\sigma(\mathbf{S}_i)^{1/\tau} \right), \quad (1)$$

where \mathbf{T}_i and \mathbf{S}_i (both have been adjusted to the same dimension via 1×1 convolution and up-/down-sampling operations) are the i -th feature/logit item extracted from \mathbb{T} and \mathbb{S} , respectively. $\sigma(\cdot)$ is the softmax normalization along the channel dimension. $\tau \in \mathbb{R}_+$ is the temperature scaling coefficient. M denotes the learning objective of \mathbf{T}_i and \mathbf{S}_i .

Following [55, 90], to simplify temperature scaling effectively, we use $\mathbf{T}_i/\mathbf{S}_i$ divided by τ to achieve the same effect. In addition to the cross-entropy loss, other loss functions are also commonly used for KD, including KL divergence loss and mean square error loss [44, 45, 97].

Although the current KD methods have achieved promising results in general vision tasks, in SS, existing methods have not considered the specific feature understanding over the object boundary and connecting regions, resulting in a performance gap. To address this problem, we will propose two targeted KD schemes for SS based on the observations of the failure cases of small models in Figure 1 to further enhance their performance.

4. Boundary and Relation Distillation (BRD)

4.1. Overview

Figure 2 provides an overview of the network architecture for our proposed BRD scheme for SS. The architecture consists of a teacher network \mathbb{T} , which is a large network that has been trained, and a small student network \mathbb{S} that is waiting to be trained. The input is an arbitrary RGB image, and the output is a segmentation mask \mathbf{Y} that predicts each pixel with a specific class label. To simplify this figure and emphasize our contributions, we omitted the SS loss \mathcal{L}_{SS} for \mathbb{S} , as well as the concatenation operation along the channel dimension with the output channel size of 256 after a 3×3 conv for \mathbf{T}_i and \mathbf{S}_i . The concatenated features are defined as \mathbf{T}^c and \mathbf{S}^c , respectively. It should be noted that both \mathbf{T}_i and \mathbf{S}_i that are concatenated have been uniformly resized into $1/8$ of the image’s spatial size. In the training stage, we propose targeted *boundary distillation* and *relation distillation* schemes that are tailored for SS tasks. Specifically, *boundary distillation* synthesizes explicit object boundaries \mathbf{T}^B and \mathbf{S}^B from \mathbf{T}^c and \mathbf{S}^c , respectively, thereby the completeness of \mathbb{S} ’s results in the boundary regions can be enhanced. Concurrently, *relation distillation* transfers implicit object relation \mathbf{T}^R and \mathbf{S}^R from \mathbb{T} to \mathbb{S} by using pixel-level self-relations, ensuring that \mathbb{S} ’s results have strong target region connectivity. Only \mathbb{S} is used in the inference stage, so there are no computational overheads of our BRD.

4.2. Boundary Distillation

The class-level object boundary is defined as a set of arbitrary pixel pairs from the given image, where the boundary between pairwise pixels has a value of 1 if they belong to different classes (*i.e.*, indicating the presence of a boundary). Conversely, if the pairwise pixels belong to the same class, the boundary between them has a value of 0 (*i.e.*, indicating the absence of a boundary) [1, 4, 15]. Moreover, this attribute also exists in the hierarchical features/logits extracted by the backbone [10, 23]. Therefore, we can use the class-level semantic affinity between arbitrary pairwise

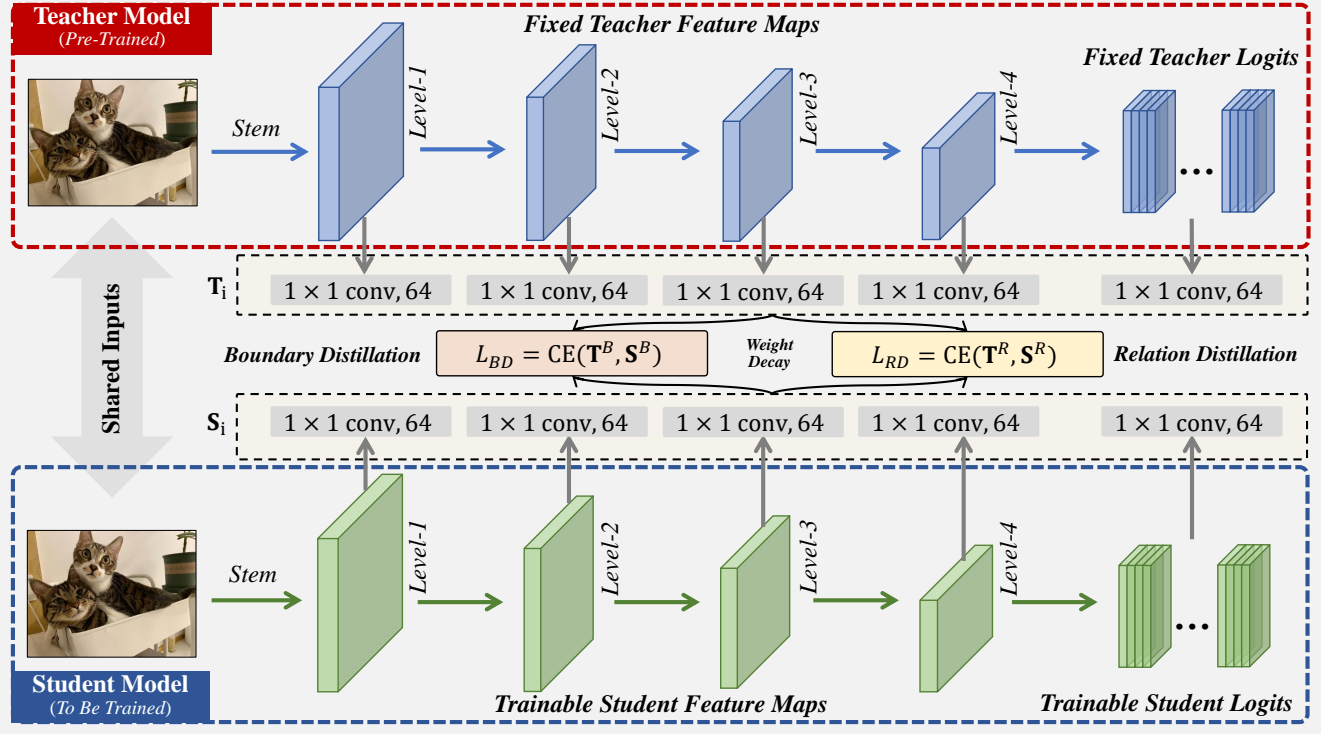


Figure 2. Overall architecture of our proposed boundary and relation distillation strategy for semantic segmentation, consisting of *boundary distillation* and *relation distillation*. The *boundary distillation* synthesizes explicit object boundaries from the hierarchical backbone features. Concurrently, the *relation distillation* transfers implicit relation information from the teacher model \mathbb{T} to the student model \mathbb{S} via pixel-level self-relations. “CE(\cdot)” denotes the cross entropy loss.

pixels from \mathbf{T}^c or \mathbf{S}^c to obtain the object boundaries [2, 56] of \mathbb{T} or \mathbb{S} . Based on which, \mathbf{T}^B can be expressed as:

$$\mathbf{T}^B = 1 - \max_{i,j \in N} \mathcal{B}(\text{Conv}_{1 \times 1}(\mathbf{T}_i^c), \text{Conv}_{1 \times 1}(\mathbf{T}_j^c)), \quad (2)$$

where \mathbf{T}_i^c and \mathbf{T}_j^c are two arbitrary pixel items from \mathbf{T}^c . $\text{Conv}_{1 \times 1}$ denotes a 1×1 convolution layer that is used to compress the channel dimension, where the input channel size is 256 and output channel size is 1. N denotes all pixel items on the line between \mathbf{T}_i^c and \mathbf{T}_j^c . $\mathcal{B}(\cdot)$ denotes the operation that determines the class-level object boundary values, which outputs either 1 or 0. \mathbf{S}^B can be obtained analogously. Based on \mathbf{T}^B and \mathbf{S}^B , our *boundary distillation* loss can be formulated as:

$$\mathcal{L}_{BD} = -\tau^2 \sum_{i \in M} \rho(\mathbf{T}_i^B)^{1/\tau} \log(\rho(\mathbf{S}_i^B)^{1/\tau}), \quad (3)$$

where ρ denotes the softmax normalization along the spatial dimension. By Eq. (3), \mathbb{T} ’s accurate prediction of the object boundary region can be transferred into \mathbb{S} , thereby addressing its issue of maintaining boundary region completeness.

4.3. Relation Distillation

Elaborate pixel-level self-relations, as demonstrated in [7, 39, 67], are beneficial for learning structured information

across spatial dimensions in dense prediction tasks [34, 40]. In this paper, we also adopt this strategy to address the issue of fragmented target regions in SS. We consider this strategy as a bridge in the KD process that enhances the feature representations of \mathbb{S} . The key benefit of our method is that it avoids the increase in model complexity and computational parameters in inference that is typically associated with current methods [40, 45]. For the concatenated features \mathbf{T}^c of \mathbb{T} , its self-relation \mathbf{T}^R can be formulated as:

$$\mathbf{T}^R = \sigma\left(\frac{O(\mathbf{T}^c)^T \cdot O(\mathbf{T}^c)}{\sqrt{d}}\right) / \tau \in \mathbb{R}^{hw \times hw}, \quad (4)$$

where $O(\cdot)$ denotes the region-aligned operation as in [39, 73], and T denotes the matrix transpose operation. d is the channel size of \mathbf{T}^c , which is 256 in our method. h and w denotes the height and width of \mathbf{T}^c , respectively. \mathbf{S}^R of \mathbb{S} can also be obtained analogously. Therefore, the *relation distillation* then can be expressed as:

$$\mathcal{L}_{RD} = -\tau^2 \sum_{k \in hw \times hw} \sigma(\mathbf{T}_k^R)^{1/\tau} \log(\sigma(\mathbf{S}_k^R)^{1/\tau}), \quad (5)$$

where $k = (1, 2, \dots, hw \times hw)$ is the index item. \mathbf{T}_k^R and \mathbf{S}_k^R denotes the k -th item in \mathbf{T}^R and \mathbf{S}^R , respectively.

4.4. Overall Loss Function

With the *boundary distillation* loss \mathcal{L}_{BD} and the *relation distillation* loss \mathcal{L}_{RD} , the total loss can be expressed as:

$$\mathcal{L} = \mathcal{L}_{SS} + \alpha\mathcal{L}_{BD} + \beta\mathcal{L}_{RD}, \quad (6)$$

where α and β are two weights used to balance different loss functions. Empirically, these weights have a significant impact on the performance of SS, and unreasonable weight settings may even lead to model collapse during training. To this end, inspired by previous work [59, 77], to enhance the dependence of \mathbb{S} on ground truth labels, we incorporate a weight-decay strategy that promotes a greater focus on \mathcal{L}_{SS} as the training epoch increases. To implement this strategy, we first initialize a time function as follows:

$$r(t) = 1 - (t - 1)/t_{\max}, \quad (7)$$

where $t = (1, 2, \dots, t_{\max})$ denotes the current training epoch and t_{\max} is the maximum training epoch. In training, we control the dependence of \mathcal{L} on \mathcal{L}_{BD} and \mathcal{L}_{RD} by using $r(t)$. Therefore, Eq. (6) can be formulated as:

$$\mathcal{L} = \mathcal{L}_{SS} + r(t)\alpha\mathcal{L}_{BD} + r(t)\beta\mathcal{L}_{RD}. \quad (8)$$

5. Experiments

5.1. Datasets and Evaluation Metrics

Datasets. In our work, we perform extensive experiments, including ablation studies, to demonstrate the superior performance of the proposed BRD on four challenging SS datasets, namely Pascal VOC 2012 [21], Cityscapes [16], ADE20K [100], and COCO-Stuff 10K [5]. Due to page limitations, the details of these datasets will be given in the supplementary material. For data augmentation, random horizontal flip, brightness jittering and random scaling within the range of $[0.5, 2]$ are used in training as in [45, 68, 87]. All the inference results are obtained at single scale.

Evaluation metrics. The commonly adopted metrics such as intersection-over-union (mIoU) and pixel-level accuracy (PixelAcc.) are used to assess the accuracy. In addition, to evaluate efficiency, parameters (Params.) and floating point operations (FLOPs) are also considered.

5.2. Implementation Details

Baseline models. For a fair result comparison [45, 68, 97], we select the classic PSPNet [93] and DeepLabV3 Plus [13] with ResNet [31] as their backbones for the teacher models. The student models are compact PSPNet and DeepLabV3+ with ResNet-38, ResNet-18_(0.5) and ResNet-18_(1.0) [31]. In addition, to validate the effectiveness of our method on cross-architecture scenarios, following [45, 68, 75], we also employ MobileNetV2 [43] and EfficientNet-B1 [60] as the

Table 1. Result comparisons with state-of-the-art methods on the *val* set of Pascal VOC 2012 [21].

Methods	<i>val</i> (%)	Params. (M)
CRF-RNN [95]	72.90	94.0
DeepLab-LargeFOV [11]	75.54	82.5
DeepLabV3 [12]	78.51	81.9
DANet [24]	80.40	83.1
<hr/>		
T: PSPNet-101 [93]	77.82	70.43
S: PSPNet-18 _(1.0) [93]	70.78	15.24
+ BRD	74.65 ^{+3.87}	15.24
S: PSPNet-18 _(0.5) [93]	54.82	3.84
+ BRD	60.67 ^{+5.85}	3.84
S: PSPNet-38 [93]	72.65	58.61
+ BRD	75.15 ^{+2.50}	58.61
S: EfficientNet-B1 [60]	69.28	6.70
+ BRD	73.81 ^{+4.53}	6.70

student models. The teacher-student pairs will be detailedly introduced in the experimental tables.

Training details. In accordance with the standard practices outlined in [32, 45, 68], all teacher models are pre-trained on the corresponding dataset before their parameters are fixed in KD. During this process, only the parameters of the student models are updated. For the student models, the SGD is used as the optimizer with the “poly” learning rate strategy. The initial learning rate is set to 0.01, with a power of 0.9. To ensure fairness in the experimental comparisons, the batch size is set to 8 and t_{\max} is set to 40,000. As in [55, 87], τ is initialized to 1 and is multiplied by a scaling factor of 1.05 whenever the range of values (across all feature items in a given minibatch) exceeds 0.5. Following [59, 68, 77], α and β is set to 10 and 50, respectively. To accommodate the local hardware limitations, training samples are cropped into the uniform size of 513×513 , and zero padding is used if needed. All experiments are implemented on the MMRazor framework¹ under the PyTorch platform [53] using 4 NVIDIA GeForce RTX 3090 GPUs. Unless otherwise specified, all other experimental settings followed those of the baselines.

5.3. Comparisons with State-of-the-Arts

Results on Pascal VOC 2012 [21]. We first evaluate the effectiveness of BRD on the *val* set of Pascal VOC 2012. PSPNet-101 [93] is utilized as the teacher network. Results on different student models are given in Table 1. From this table, we can observe that: 1) BRD can boost the accuracy of different types of student models, including variants of the same architecture (*i.e.*, PSPNet-38 with 2.50% mIoU \uparrow , PSPNet-18_(1.0) with 3.87% mIoU \uparrow and PSPNet-18_(0.5) with 5.85% mIoU \uparrow) and different network architec-

¹<https://github.com/open-mmlab/mmrazor>

Table 2. Result comparisons with state-of-the-art methods on the *val* set of Cityscapes [16] dataset. Our model is only trained on the finely-annotated training samples.

Methods	<i>val</i> (%)	Params. (M)	FLOPs (G)
ICNet [94]	67.9	26.48	28.3
RefineNet [41]	72.6	118.13	525.7
OCNet [81]	80.7	62.58	548.5
HRNet [58]	81.1	65.90	747.3
<hr/>			
T: PSPNet-101 [93]	78.56	70.43	574.9
S: PSPNet-18 _(1.0) [93]	69.10	15.24	128.2
+ BRD	74.92 ^{+5.81}	15.24	128.2
S: PSPNet-18 _(0.5) [93]	55.40	3.84	33.4
+ BRD	61.62 ^{+6.22}	3.84	33.4
S: PSPNet-38 [93]	71.26	47.4	54.3
+ BRD	73.56 ^{+2.30}	47.4	54.3
S: EfficientNet-B1 [60]	60.40	6.70	9.9
+ BRD	63.91 ^{+3.51}	6.70	9.9

Table 3. Result comparisons with state-of-the-art methods on the *val* set of ADE20K [100] dataset.

Methods	mIoU (%)	Pixel Acc. (%)	Params. (M)
SegNet [3]	21.64	71.00	29.46
FCN [48]	29.39	71.32	134.50
DilatedNet-50 [71]	34.28	76.35	62.74
DeepLabV3 [12]	43.28	82.60	71.29
<hr/>			
T: PSPNet-101 [93]	42.19	80.59	70.43
S: ResNet-18 _(1.0) [93]	33.82	76.05	15.24
+ BRD	37.62 ^{+3.80}	79.33	15.24
S: ResNet-18 _(0.5) [93]	25.16	55.31	3.84
+ BRD	29.02 ^{+3.86}	58.88	3.84
S: ESPNet [50]	20.13	70.54	0.36
+ BRD	23.65 ^{+3.52}	74.22	0.36
S: MobileNetV2 [43]	33.64	74.38	8.30
+ BRD	36.59 ^{+2.95}	77.25	8.30

tures (*i.e.*, EfficientNet-B1 [60] with 4.53% mIoU \uparrow). This indicates that our method has a strong generalization application capacity. 2) Compared to the state-of-the-art methods without, our method can achieve very competitive accuracy with fewer parameters. For example, under the help of BRD, PSPNet-18_(1.0) [93] achieves 92.85% accuracy (*i.e.*, 74.65% mIoU) of DANet (*i.e.*, 80.40% mIoU) [24], but with only 18.34% (*i.e.*, 15.24M) of its parameters (*i.e.*, 83.1M).

Results on Cityscapes [16]. Our method is then evaluated on the *val* set of Cityscapes. We selected the same teacher and student models as those used on Pascal VOC 2012 [21]. Experimental results are given in Table 2. We can observe that our BRD can still improve the accuracy of different student models, *i.e.*, 5.81% mIoU \uparrow on PSPNet-18_(1.0), 6.22% mIoU \uparrow on PSPNet-18_(0.5), 2.30% mIoU \uparrow on PSPNet-38, and 3.51% mIoU \uparrow on EfficientNet-B1 [60]. Besides, from

Table 4. Result comparisons with state-of-the-art methods on the *test* set of COCO-Stuff 10K [5].

Methods	<i>test</i> (%)	FLOPs (G)
DeepLab-V2 [11]	34.4	45.6
OCRNet [82]	39.5	209.2
DANet [24]	39.7	67.3
StructToken [40]	49.1	>400
SegViT [84]	50.3	383.9
<hr/>		
T: DeepLabV3 Plus-101 [13]	33.10	366.9
S: DeepLabV3 Plus-18 [13]	26.33	92.3
+ BRD	29.22 ^{+2.89}	92.3
S: MobileNetV2 [43]	26.29	1.4
+ BRD	28.31 ^{+2.02}	1.4

Table 1 and 2, we can observe that compared to the results on other student models, BRD has a smaller performance gain on PSPNet-38 (*i.e.*, 2.50% mIoU \uparrow and 2.30% mIoU \uparrow). This may be because there is a small accuracy gap between PSPNet-38 and PSPNet-101 [93], which means PSPNet-101 cannot provide very beneficial boundary and relation information for the student model PSPNet-38.

Results on ADE20K [100]. We also validate our BRD on the *val* set of ADE20K. In addition to PSPNet-18_(1.0) and PSPNet-18_(0.5), we also employ ESPNet [50] and MobileNetV2 [43] as the student models to validate the effectiveness of BRD across network architectures. The experimental results in Table 3 declare that BRD has consistent improvement not only on student models with the same structure (*i.e.*, 3.80% mIoU \uparrow on PSPNet-18_(1.0) and 3.86% mIoU \uparrow on PSPNet-18_(0.5)) when applied to datasets with a larger class size (*i.e.*, 150 in ADE20K [100]), but also demonstrates consistent accuracy gains across different student architectures (*i.e.*, 3.52% mIoU \uparrow on ESPNet and 2.95% mIoU \uparrow on MobileNetV2).

Results on COCO-Stuff 10K [5]. Experimental results on the *test* set of COCO-Stuff 10K is given in Table 4, where the teacher model is DeepLabV3 Plus-101 [13] and the student models are DeepLabV3 Plus-18 and MobileNetV2 [43]. It can be observed that our BRD still yields accuracy improvements for different student models (*i.e.*, 2.89% mIoU \uparrow on DeepLabV3 Plus-18 and 2.02% mIoU \uparrow on MobileNetV2) when used with DeepLabV3 Plus-101 as the teacher model. Furthermore, our method achieves competitive results compared to the strong SegViT [84] model. Under the implementation of BRD, DeepLabV3 Plus-18 finally achieves 29.22% (*i.e.*, 58.09% of SegViT) mIoU and has only 92.3G (*i.e.*, 24.0% of SegViT) FLOPs.

Visualized comparisons. The visualized results obtained from the conducted experiments are presented in Figure 3, where we compare the results before and after using BRD on the student model, as well as the results of the teacher model and the results of state-of-the-art methods. The visu-

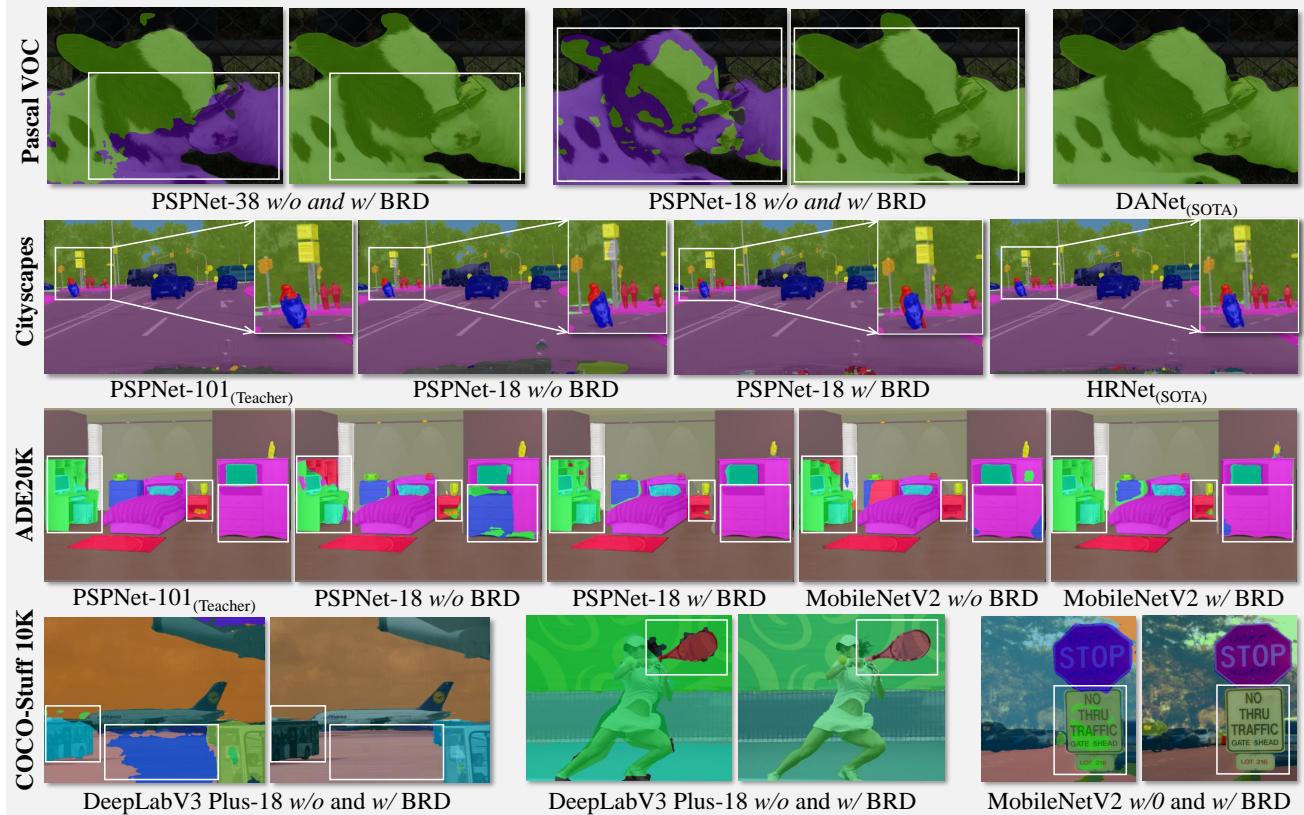


Figure 3. Visualizations on the conducted datasets. “w/o” means without and “w/” means with, indicating whether BRD is NOT implemented or implemented on the corresponding baseline. The white bounding boxes highlight the regions where our method predicts better.

Table 5. Ablation study results on the *val* set of Pascal VOC 2012 [21]. “WD” denotes the weight-decay strategy in Sec. 4.4.

			T: PSPNet-101 [93]	77.82	70.43	411.6
			S: PSPNet-18 _(1.0) [93]	70.78	15.24	106.2
\mathcal{L}_{BD}	\mathcal{L}_{RD}	WD	mIoU (%)	Params. (M)	FLOPs (G)	
✓	✗	✗	71.69 ^{+0.91}	15.24	106.2	
✗	✓	✗	72.55 ^{+1.77}	15.24	106.2	
✓	✓	✗	73.98 ^{+3.20}	15.24	106.2	
✓	✓	✓	74.65 ^{+3.87}	15.24	106.2	

alized results validate that BRD yields significant improvements in terms of boundary region completeness and object region connectivity. For example, the “cow” in Pascal VOC 2012 [21], the “guidepost” in Cityscapes [16], the “desk” and the “TV bench” in ADE20K [100], the “bus”, the “tennis racket”, and the “guideboard” in COCO-Stuff 10K [5]. Besides, compared to the state-of-the-art methods (*i.e.*, DANet [24] and HRNet [58]) without KD on Pascal VOC 2012 and Cityscapes, although our method is not as good as theirs in overall performance, our model achieves better predictions on object boundaries and even small objects, which validates the effectiveness of boundary distillation and relation distillation. For example, the “cow’s ear” and the “person’s leg”.

5.4. Ablation Study

This section investigates the effectiveness of each component, the superiority performance, and the effectiveness of joint implementation of our BRD and other KD methods. PSPNet-101 [93] is employed as the teacher model, while PSPNet-18_(1.0) serves as the student model. The results are reported on the *val* set of Pascal VOC 2012 [21].

Effectiveness of each component. Table 5 shows the accuracy by adding each component of BRD into the baseline model. It can be observed that incorporating these different components consistently improves the accuracy, indicating the effectiveness of these components. In particular, adding \mathcal{L}_{BD} resulted in a mIoU gain of 0.91%, which may be attributed to the fact that the boundary regions within the objects are relatively small in proportion [87]. Besides, with only the implementation of \mathcal{L}_{BD} and \mathcal{L}_{RD} , our model can achieve the competitive 73.98% mIoU with 3.20% mIoU improvements, outperforming the sum of the individual improvements from adding \mathcal{L}_{BD} and \mathcal{L}_{RD} separately, which verifies the importance of boundaries and relations in the SS tasks. Building upon \mathcal{L}_{BD} and \mathcal{L}_{RD} , adding the weight-decay strategy can further bring 0.57% mIoU, which verifies the weight importance of different losses on SS.

Table 6. Result comparisons with other KD methods, and the effectiveness of joint implementation of our BRD and other KD methods on the *val* set of Pascal VOC 2012 [21]. “ \ddagger ” denotes our re-implemented result based on the released codes.

T: PSPNet-101 [93]		77.82
S: PSPNet-18 _(1.0) [93]		70.78
Methods	Pub. Year	mIoU (%)
+ KD [32]	arXiv’15	71.28 \ddagger +0.50
+ SKD [45]	CVPR’19	73.05 +2.27
+ SR [87]	ICCV’21	72.18 +1.40
+ SCKD [101]	ICCV’21	72.33 +1.55
+ CIRKD [75]	CVPR’22	73.57 \ddagger +2.79
+ IFD [14]	NeurIPS ’22	73.88 \ddagger +3.10
+ FGKD [76]	CVPR’22	72.90 \ddagger +2.12
+ CWT [47]	ICCV’23	73.06 \ddagger +2.28
+ C2VKD [97]	arXiv’23	73.85 \ddagger +3.07
+ BRD _{ours}	submission	74.65 +3.87
+ IFVD [68]	ECCV’20	74.05 +3.27
+ IFVD [68] + BRD _{ours}	submission	74.82 +4.04
+ TAT [42]	CVPR’22	74.02 \ddagger +3.24
+ TAT [42] + BRD _{ours}	submission	74.71 +3.93
+ SSTKD [34]	CVPR’22	73.91 +3.13
+ SSTKD [34] + BRD _{ours}	submission	74.52 +3.74

Superiority performance of BRD. Compared to the current feature-based and logit-based KD methods, in the top half of Table 6, we can observe that our BRD surpasses these methods, which boosts the baseline model by 3.87% mIoU. In particular, compared to the state-of-the-art KD methods on SS, our BRD method outperforms IFVD [68], TAT [42], and SSTKD [34] by 0.50%, 0.63%, and 0.74%, respectively. This result confirms that task-specific knowledge transfer is indeed more effective in practice compared to general knowledge transfer as we mentioned in Sec. 1.

Effectiveness of joint implementation of BRD and other KD methods. The experimental results on the joint implementation of our BRD and three state-of-the-art KD methods on the *val* set of Pascal VOC 2012 [21] are presented in the lower half of Table 6. Some of the results are re-implemented by us due to inconsistencies in experimental settings and are marked with \ddagger . It can be observed that, on top of BRD, further adding IFVD [68] and TAT [42] still yields consistent performance gains, with mIoU improvements of 0.17% and 0.06%, respectively. This can be attributed to the fact that BRD contains object relation information that is not present in these methods, further demonstrating the importance of relation information for SS. However, adding SSTKD [34] on top of BRD resulted in a performance decrease (*i.e.*, 0.13% mIoU \downarrow). We guess that this may be because SSTKD [34] uses coarse textures from the image, which is non-semantic and contains some noise relative to the extracted semantic boundaries.

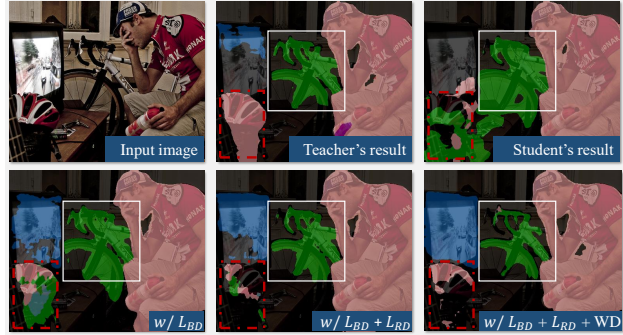


Figure 4. Visualized comparisons between the baseline model [93] and the results obtained by adding different components of BRD. “WD” denotes the used weight-decay strategy in Sec. 4.4. The teacher model and the student model denotes PSPNet-101 [93] and PSPNet-18_(1.0) [93], respectively. “w/” denotes with the corresponding implementation. Samples are from the Pascal VOC 2012 [21] dataset.

Visualization results. We employ visualizations as a means of verifying the efficacy of incorporating BRD items (*i.e.*, \mathcal{L}_{BD} , \mathcal{L}_{RD} , and the weight-decay strategy) incrementally into the baseline model. The obtained results are presented in Figure 4, which demonstrate that the inclusion of \mathcal{L}_{BD} and \mathcal{L}_{RD} in a sequential manner leads to enhanced boundary regions and object connectivity. For example, the “bike handlebar”. Moreover, the integration of the the weight-decay strategy, *i.e.*, “WD”, results in further improvement in the overall segmentation predictions. We also highlighted the regions of prediction failure using red dashed bounding boxes. We can observe that although our BRD significantly improves the prediction quality of these regions compared to the student model’s results, there are still some incomplete predictions. This case may be caused by the spurious correlation between the “helmet” and “person” in the dataset, which can be eliminated through causal intervention to improve the prediction quality [83, 86].

6. Conclusion

In this paper, we proposed a targeted boundary and relation distillation (BRD) strategy to address the performance gap between large and small semantic segmentation models. The proposed BRD effectively maintained boundary region completeness and preserved target region connectivity, resulting in improved accuracy across multiple challenging datasets without increasing inference costs. As a general knowledge distillation method, we intend to explore the effectiveness of BRD in other dense prediction tasks and architectures, such as instance segmentation and panoptic segmentation, as well as those based on Vision Transformers, in the future. Furthermore, we will explore the potential of combining BRD with visual foundation models, such as the segment anything model, to further improve the performance of small semantic segmentation models.

References

- [1] Jiwoon Ahn and Suha Kwak. Learning pixel-level semantic affinity with image-level supervision for weakly supervised semantic segmentation. In *CVPR*, pages 4981–4990, 2018. [3](#)
- [2] Jiwoon Ahn, Sunghyun Cho, and Suha Kwak. Weakly supervised learning of instance segmentation with inter-pixel relations. In *CVPR*, pages 2209–2218, 2019. [4](#)
- [3] Vijay Badrinarayanan, Alex Kendall, and Roberto Cipolla. Segnet: A deep convolutional encoder-decoder architecture for image segmentation. *IEEE T-PAMI*, 39(12):2481–2495, 2017. [6](#)
- [4] Gedas Bertasius, Lorenzo Torresani, Stella X Yu, and Jianbo Shi. Convolutional random walk networks for semantic image segmentation. In *CVPR*, pages 858–866, 2017. [3](#)
- [5] Holger Caesar, Jasper Uijlings, and Vittorio Ferrari. Coco-stuff: Thing and stuff classes in context. In *CVPR*, pages 1209–1218, 2018. [2](#), [5](#), [6](#), [7](#)
- [6] Hu Cao, Yueyue Wang, Joy Chen, Dongsheng Jiang, Xiaopeng Zhang, Qi Tian, and Manning Wang. Swin-unet: Unet-like pure transformer for medical image segmentation. In *ECCV*, pages 205–218, 2022. [1](#), [2](#)
- [7] Mathilde Caron, Hugo Touvron, Ishan Misra, Hervé Jégou, Julien Mairal, Piotr Bojanowski, and Armand Joulin. Emerging properties in self-supervised vision transformers. In *ICCV*, pages 9650–9660, 2021. [4](#)
- [8] Guobin Chen, Wongun Choi, Xiang Yu, Tony Han, and Manmohan Chandraker. Learning efficient object detection models with knowledge distillation. In *NeurIPS*, 2017. [3](#)
- [9] Jieneng Chen, Yongyi Lu, Qihang Yu, Xiangde Luo, Ehsan Adeli, Yan Wang, Le Lu, Alan L Yuille, and Yuyin Zhou. Transunet: Transformers make strong encoders for medical image segmentation. *arXiv*, 2021. [2](#)
- [10] Liyi Chen, Weiwei Wu, Chenchen Fu, Xiao Han, and Yuntao Zhang. Weakly supervised semantic segmentation with boundary exploration. In *ECCV*, pages 347–362, 2020. [3](#)
- [11] Liang-Chieh Chen, George Papandreou, Iasonas Kokkinos, Kevin Murphy, and Alan L Yuille. Deeplab: Semantic image segmentation with deep convolutional nets, atrous convolution, and fully connected crfs. *IEEE T-PAMI*, 40(4): 834–848, 2017. [5](#), [6](#)
- [12] Liang-Chieh Chen, George Papandreou, Florian Schroff, and Hartwig Adam. Rethinking atrous convolution for semantic image segmentation. *arXiv*, 2017. [5](#), [6](#)
- [13] Liang-Chieh Chen, Yukun Zhu, George Papandreou, Florian Schroff, and Hartwig Adam. Encoder-decoder with atrous separable convolution for semantic image segmentation. In *ECCV*, pages 801–818, 2018. [5](#), [6](#)
- [14] Yudong Chen, Sen Wang, Jiajun Liu, Xuwei Xu, Frank de Hoog, and Zi Huang. Improved feature distillation via projector ensemble. In *NeurIPS*, pages 12084–12095, 2022. [8](#)
- [15] Yanhua Cheng, Rui Cai, Zhiwei Li, Xin Zhao, and Kaiqi Huang. Locality-sensitive deconvolution networks with gated fusion for rgb-d indoor semantic segmentation. In *CVPR*, pages 3029–3037, 2017. [3](#)
- [16] Marius Cordts, Mohamed Omran, Sebastian Ramos, Timo Rehfeld, Markus Enzweiler, Rodrigo Benenson, Uwe Franke, Stefan Roth, and Bernt Schiele. The cityscapes dataset for semantic urban scene understanding. In *CVPR*, pages 3213–3223, 2016. [2](#), [5](#), [6](#), [7](#)
- [17] Kaiwen Cui, Yingchen Yu, Fangneng Zhan, Shengcai Liao, Shijian Lu, and Eric P Xing. Kd-dlgn: Data limited image generation via knowledge distillation. In *CVPR*, pages 3872–3882, 2023. [1](#), [3](#)
- [18] Pingcheng Dong, Zhuoyu Chen, Zhuoao Li, Yuzhe Fu, Lei Chen, and Fengwei An. A 4.29 nj/pixel stereo depth coprocessor with pixel level pipeline and region optimized semi-global matching for iot application. *IEEE TCS*, 69(1):334–346, 2021. [2](#)
- [19] Pingcheng Dong, Zhuoyu Chen, Ke Li, Lei Chen, Kwang-Ting Cheng, and Fengwei An. A 1920× 1080 129fps 4.3 pj/pixel stereo-matching processor for pico aerial vehicles. In *ESSCIRC*, pages 345–348, 2023. [2](#)
- [20] Xiaoyi Dong, Jianmin Bao, Dongdong Chen, Weiming Zhang, Nenghai Yu, Lu Yuan, Dong Chen, and Baining Guo. Cswin transformer: A general vision transformer backbone with cross-shaped windows. In *CVPR*, pages 12124–12134, 2022. [2](#)
- [21] Mark Everingham, Luc Van Gool, Christopher KI Williams, John Winn, and Andrew Zisserman. The pascal visual object classes (voc) challenge. *IJCV*, 88:303–338, 2010. [2](#), [5](#), [6](#), [7](#), [8](#)
- [22] Haoqi Fan, Bo Xiong, Karttikeya Mangalam, Yanghao Li, Zhicheng Yan, Jitendra Malik, and Christoph Feichtenhofer. Multiscale vision transformers. In *ICCV*, pages 6824–6835, 2021. [2](#)
- [23] Jordi Freixenet, Xavier Munoz, David Raba, Joan Martí, and Xavier Cufí. Yet another survey on image segmentation: Region and boundary information integration. In *ECCV*, pages 408–422, 2002. [3](#)
- [24] Jun Fu, Jing Liu, Haijie Tian, Yong Li, Yongjun Bao, Zhiwei Fang, and Hanqing Lu. Dual attention network for scene segmentation. In *CVPR*, pages 3146–3154, 2019. [1](#), [5](#), [6](#), [7](#)
- [25] Jianping Gou, Baosheng Yu, Stephen J Maybank, and Dacheng Tao. Knowledge distillation: A survey. *IJCV*, 129:1789–1819, 2021. [1](#), [3](#)
- [26] Jianping Gou, Xiangshuo Xiong, Baosheng Yu, Lan Du, Yibing Zhan, and Dacheng Tao. Multi-target knowledge distillation via student self-reflection. *IJCV*, pages 1–18, 2023. [3](#)
- [27] Jianyuan Guo, Kai Han, Han Wu, Yehui Tang, Xinghao Chen, Yunhe Wang, and Chang Xu. Cmt: Convolutional neural networks meet vision transformers. In *CVPR*, pages 12175–12185, 2022. [2](#)
- [28] Qiushan Guo, Xinjiang Wang, Yichao Wu, Zhipeng Yu, Ding Liang, Xiaolin Hu, and Ping Luo. Online knowledge distillation via collaborative learning. In *CVPR*, pages 11020–11029, 2020. [3](#)
- [29] Kai Han, Yunhe Wang, Hanting Chen, Xinghao Chen, Jianyuan Guo, Zhenhua Liu, Yehui Tang, An Xiao, Chungjing Xu, Yixing Xu, et al. A survey on vision transformer. *IEEE T-PAMI*, 45(1):87–110, 2022. [2](#)

- [30] Zhiwei Hao, Yong Luo, Han Hu, Jianping An, and Yonggang Wen. Data-free ensemble knowledge distillation for privacy-conscious multimedia model compression. In *ACM MM*, pages 1803–1811, 2021. [1](#)
- [31] Kaiming He, Xiangyu Zhang, Shaoqing Ren, and Jian Sun. Deep residual learning for image recognition. In *CVPR*, pages 770–778, 2016. [5](#)
- [32] Geoffrey Hinton, Oriol Vinyals, and Jeff Dean. Distilling the knowledge in a neural network. *arXiv*, 2015. [1](#), [3](#), [5](#), [8](#)
- [33] Zilong Huang, Xinggang Wang, Lichao Huang, Chang Huang, Yunchao Wei, and Wenyu Liu. Cnet: Criss-cross attention for semantic segmentation. In *CVPR*, pages 603–612, 2019. [2](#)
- [34] Deyi Ji, Haoran Wang, Mingyuan Tao, Jianqiang Huang, Xian-Sheng Hua, and Hongtao Lu. Structural and statistical texture knowledge distillation for semantic segmentation. In *CVPR*, pages 16876–16885, 2022. [4](#), [8](#)
- [35] Mingi Ji, Seungjae Shin, Seunghyun Hwang, Gibeom Park, and Il-Chul Moon. Refine myself by teaching myself: Feature refinement via self-knowledge distillation. In *CVPR*, pages 10664–10673, 2021. [3](#)
- [36] Zhenglun Kong, Peiyang Dong, Xiaolong Ma, Xin Meng, Wei Niu, Mengshu Sun, Xuan Shen, Geng Yuan, Bin Ren, Hao Tang, et al. Spvit: Enabling faster vision transformers via latency-aware soft token pruning. In *ECCV*, pages 620–640, 2022. [2](#)
- [37] Seunghyun Lee and Byung Cheol Song. Graph-based knowledge distillation by multi-head attention network. *arXiv*, 2019. [3](#)
- [38] Jiashi Li, Xin Xia, Wei Li, Huixia Li, Xing Wang, Xuefeng Xiao, Rui Wang, Min Zheng, and Xin Pan. Next-vit: Next generation vision transformer for efficient deployment in realistic industrial scenarios. *arXiv*, 2022. [2](#)
- [39] Zhong-Yu Li, Shanghua Gao, and Ming-Ming Cheng. Exploring feature self-relation for self-supervised transformer. *arXiv*, 2022. [4](#)
- [40] Fangjian Lin, Zhanhao Liang, Sitong Wu, Junjun He, Kai Chen, and Shengwei Tian. Structtoken: Rethinking semantic segmentation with structural prior. *IEEE T-CSVT*, 2023. [4](#), [6](#)
- [41] Guosheng Lin, Anton Milan, Chunhua Shen, and Ian Reid. Refinenet: Multi-path refinement networks for high-resolution semantic segmentation. In *CVPR*, pages 1925–1934, 2017. [1](#), [6](#)
- [42] Sihao Lin, Hongwei Xie, Bing Wang, Kaicheng Yu, Xiaojun Chang, Xiaodan Liang, and Gang Wang. Knowledge distillation via the target-aware transformer. In *CVPR*, pages 10915–10924, 2022. [8](#)
- [43] Huijun Liu. Lightnet: Light-weight networks for semantic image segmentation. *LighCNeC. html*, 2018. [5](#), [6](#)
- [44] Ruiping Liu, Kailun Yang, Alina Roitberg, Jiaming Zhang, Kunyu Peng, Huayao Liu, and Rainer Stiefelhagen. Transkd: Transformer knowledge distillation for efficient semantic segmentation. *arXiv*, 2022. [3](#)
- [45] Yifan Liu, Ke Chen, Chris Liu, Zengchang Qin, Zhenbo Luo, and Jingdong Wang. Structured knowledge distillation for semantic segmentation. In *CVPR*, pages 2604–2613, 2019. [1](#), [3](#), [4](#), [5](#), [8](#)
- [46] Ze Liu, Yutong Lin, Yue Cao, Han Hu, Yixuan Wei, Zheng Zhang, Stephen Lin, and Baining Guo. Swin transformer: Hierarchical vision transformer using shifted windows. In *ICCV*, pages 10012–10022, 2021. [2](#)
- [47] Ziwei Liu, Yongtao Wang, Xiaojie Chu, Nan Dong, Shengxiang Qi, and Haibin Ling. A simple and generic framework for feature distillation via channel-wise transformation. In *ICCV Workshop*, pages 1129–1138, 2023. [8](#)
- [48] Jonathan Long, Evan Shelhamer, and Trevor Darrell. Fully convolutional networks for semantic segmentation. In *CVPR*, pages 3431–3440, 2015. [1](#), [2](#), [3](#), [6](#)
- [49] Xiaofeng Mao, Gege Qi, Yuefeng Chen, Xiaodan Li, Ranjie Duan, Shaokai Ye, Yuan He, and Hui Xue. Towards robust vision transformer. In *CVPR*, pages 12042–12051, 2022. [2](#), [3](#)
- [50] Sachin Mehta, Mohammad Rastegari, Anat Caspi, Linda Shapiro, and Hannaneh Hajishirzi. Espnet: Efficient spatial pyramid of dilated convolutions for semantic segmentation. In *ECCV*, pages 552–568, 2018. [6](#)
- [51] Hyeonwoo Noh, Seunghoon Hong, and Bohyung Han. Learning deconvolution network for semantic segmentation. In *ICCV*, pages 1520–1528, 2015. [2](#)
- [52] Peyman Passban, Yimeng Wu, Mehdi Rezagholizadeh, and Qun Liu. Alp-kd: Attention-based layer projection for knowledge distillation. In *AAAI*, pages 13657–13665, 2021. [3](#)
- [53] Adam Paszke, Sam Gross, Francisco Massa, Adam Lerer, James Bradbury, Gregory Chanan, Trevor Killeen, Zeming Lin, Natalia Gimelshein, Luca Antiga, et al. Pytorch: An imperative style, high-performance deep learning library. In *NeurIPS*, 2019. [5](#)
- [54] Zhiliang Peng, Wei Huang, Shanzhi Gu, Lingxi Xie, Yaowei Wang, Jianbin Jiao, and Qixiang Ye. Conformer: Local features coupling global representations for visual recognition. In *CVPR*, pages 367–376, 2021. [2](#)
- [55] Mary Phuong and Christoph H Lampert. Distillation-based training for multi-exit architectures. In *ICCV*, pages 1355–1364, 2019. [3](#), [5](#)
- [56] Lixiang Ru, Yibing Zhan, Baosheng Yu, and Bo Du. Learning affinity from attention: End-to-end weakly-supervised semantic segmentation with transformers. In *CVPR*, pages 16846–16855, 2022. [4](#)
- [57] Robin Strudel, Ricardo Garcia, Ivan Laptev, and Cordelia Schmid. Segmenter: Transformer for semantic segmentation. In *ICCV*, pages 7262–7272, 2021. [2](#)
- [58] Ke Sun, Yang Zhao, Borui Jiang, Tianheng Cheng, Bin Xiao, Dong Liu, Yadong Mu, Xinggang Wang, Wenyu Liu, and Jingdong Wang. High-resolution representations for labeling pixels and regions. *arXiv*, 2019. [6](#), [7](#)
- [59] Ruoyu Sun, Fuhui Tang, Xiaopeng Zhang, Hongkai Xiong, and Qi Tian. Distilling object detectors with task adaptive regularization. *arXiv*, 2020. [3](#), [5](#)
- [60] Mingxing Tan and Quoc Le. Efficientnet: Rethinking model scaling for convolutional neural networks. In *ICML*, pages 6105–6114, 2019. [5](#), [6](#)
- [61] Wei-Cheng Tseng, Tsun-Hsuan Johnson Wang, Yen-Chen Lin, and Phillip Isola. Offline multi-agent reinforcement

- learning with knowledge distillation. In *NeurIPS*, pages 226–237, 2022. 3
- [62] Chi Wang, Yunke Zhang, Miaomiao Cui, Peiran Ren, Yin Yang, Xuansong Xie, Xian-Sheng Hua, Hujun Bao, and Weiwei Xu. Active boundary loss for semantic segmentation. In *AAAI*, pages 2397–2405, 2022. 1
- [63] Jiabao Wang, Yuming Chen, Zhaohui Zheng, Xiang Li, Ming-Ming Cheng, and Qibin Hou. Crosskd: Cross-head knowledge distillation for dense object detection. *arXiv*, 2023. 1, 3
- [64] Panqu Wang, Pengfei Chen, Ye Yuan, Ding Liu, Zehua Huang, Xiaodi Hou, and Garrison Cottrell. Understanding convolution for semantic segmentation. In *WACV*, pages 1451–1460, 2018. 2
- [65] Tao Wang, Li Yuan, Xiaopeng Zhang, and Jiashi Feng. Distilling object detectors with fine-grained feature imitation. In *CVPR*, pages 4933–4942, 2019. 3
- [66] Wenhai Wang, Enze Xie, Xiang Li, Deng-Ping Fan, Kaitao Song, Ding Liang, Tong Lu, Ping Luo, and Ling Shao. Pyramid vision transformer: A versatile backbone for dense prediction without convolutions. In *ICCV*, pages 568–578, 2021. 2
- [67] Xinlong Wang, Rufeng Zhang, Chunhua Shen, Tao Kong, and Lei Li. Dense contrastive learning for self-supervised visual pre-training. In *CVPR*, pages 3024–3033, 2021. 4
- [68] Yukang Wang, Wei Zhou, Tao Jiang, Xiang Bai, and Yongchao Xu. Intra-class feature variation distillation for semantic segmentation. In *ECCV*, pages 346–362, 2020. 1, 3, 5, 8
- [69] Zhendong Wang, Xiaodong Cun, Jianmin Bao, Wengang Zhou, Jianzhuang Liu, and Houqiang Li. Uformer: A general u-shaped transformer for image restoration. In *CVPR*, pages 17683–17693, 2022. 2
- [70] Haiping Wu, Bin Xiao, Noel Codella, Mengchen Liu, Xiyang Dai, Lu Yuan, and Lei Zhang. Cvt: Introducing convolutions to vision transformers. In *ICCV*, pages 22–31, 2021. 2
- [71] Tete Xiao, Yingcheng Liu, Bolei Zhou, Yuning Jiang, and Jian Sun. Unified perceptual parsing for scene understanding. In *ECCV*, pages 418–434, 2018. 6
- [72] Enze Xie, Wenhai Wang, Zhiding Yu, Anima Anandkumar, Jose M Alvarez, and Ping Luo. Segformer: Simple and efficient design for semantic segmentation with transformers. In *NeurIPS*, pages 12077–12090, 2021. 2
- [73] Wei Xie, Zimeng Zhao, Shiyang Li, Binghui Zuo, and Yanggang Wang. Nonrigid object contact estimation with regional unwrapping transformer. In *ICCV*, pages 9342–9351, 2023. 4
- [74] Kunran Xu, Lai Rui, Yishi Li, and Lin Gu. Feature normalized knowledge distillation for image classification. In *ECCV*, pages 664–680, 2020. 1, 3
- [75] Chuanguang Yang, Helong Zhou, Zhulin An, Xue Jiang, Yongjun Xu, and Qian Zhang. Cross-image relational knowledge distillation for semantic segmentation. In *CVPR*, pages 12319–12328, 2022. 1, 3, 5, 8
- [76] Zhendong Yang, Zhe Li, Xiaohu Jiang, Yuan Gong, Zehuan Yuan, Danpei Zhao, and Chun Yuan. Focal and global knowledge distillation for detectors. In *CVPR*, pages 4643–4652, 2022. 1, 8
- [77] Zhendong Yang, Ailing Zeng, Chun Yuan, and Yu Li. Effective whole-body pose estimation with two-stages distillation. In *ICCV*, pages 4210–4220, 2023. 5
- [78] Dongshuo Yin, Yiran Yang, Zhechao Wang, Hongfeng Yu, Kaiwen Wei, and Xian Sun. 1% vs 100%: Parameter-efficient low rank adapter for dense predictions. In *CVPR*, pages 20116–20126, 2023. 1
- [79] Changqian Yu, Jingbo Wang, Chao Peng, Changxin Gao, Gang Yu, and Nong Sang. Bisenet: Bilateral segmentation network for real-time semantic segmentation. In *ECCV*, pages 325–341, 2018. 1, 2
- [80] Fei Yuan, Linjun Shou, Jian Pei, Wutao Lin, Ming Gong, Yan Fu, and Daxin Jiang. Reinforced multi-teacher selection for knowledge distillation. In *AAAI*, pages 14284–14291, 2021. 3
- [81] Yuhui Yuan, Lang Huang, Jianyuan Guo, Chao Zhang, Xilin Chen, and Jingdong Wang. Ocnet: Object context network for scene parsing. *arXiv*, 2018. 6
- [82] Yuhui Yuan, Xilin Chen, and Jingdong Wang. Object-contextual representations for semantic segmentation. In *ECCV*, pages 173–190, 2020. 1, 6
- [83] Zhongqi Yue, Hanwang Zhang, Qianru Sun, and Xian-Sheng Hua. Interventional few-shot learning. In *NeurIPS*, pages 2734–2746, 2020. 8
- [84] Bowen Zhang, Zhi Tian, Quan Tang, Xiangxiang Chu, Xiaolin Wei, Chunhua Shen, et al. Segvit: Semantic segmentation with plain vision transformers. In *NeurIPS*, pages 4971–4982, 2022. 6
- [85] Chaoning Zhang, Dongshen Han, Yu Qiao, Jung Uk Kim, Sung-Ho Bae, Seungkyu Lee, and Choong Seon Hong. Faster segment anything: Towards lightweight sam for mobile applications. *arXiv*, 2023. 1, 2
- [86] Dong Zhang, Hanwang Zhang, Jinhui Tang, Xian-Sheng Hua, and Qianru Sun. Causal intervention for weakly-supervised semantic segmentation. In *NeurIPS*, pages 655–666, 2020. 1, 2, 8
- [87] Dong Zhang, Hanwang Zhang, Jinhui Tang, Xian-Sheng Hua, and Qianru Sun. Self-regulation for semantic segmentation. In *ICCV*, pages 6953–6963, 2021. 1, 2, 3, 5, 7, 8
- [88] Dong Zhang, Jinhui Tang, and Kwang-Ting Cheng. Graph reasoning transformer for image parsing. In *ACM MM*, pages 2380–2389, 2022. 1, 2, 3
- [89] Hang Zhang, Kristin Dana, Jianping Shi, Zhongyue Zhang, Xiaoang Wang, Amrith Tyagi, and Amit Agrawal. Context encoding for semantic segmentation. In *CVPR*, pages 7151–7160, 2018. 2, 3
- [90] Linfeng Zhang, Jiebo Song, Anni Gao, Jingwei Chen, Chenglong Bao, and Kaisheng Ma. Be your own teacher: Improve the performance of convolutional neural networks via self distillation. In *ICCV*, pages 3713–3722, 2019. 3
- [91] Wenqiang Zhang, Zilong Huang, Guozhong Luo, Tao Chen, Xinggang Wang, Wenyu Liu, Gang Yu, and Chunhua Shen. Topformer: Token pyramid transformer for mobile semantic segmentation. In *CVPR*, pages 12083–12093, 2022. 1, 2

- [92] Borui Zhao, Quan Cui, Renjie Song, Yiyu Qiu, and Jiajun Liang. Decoupled knowledge distillation. In *CVPR*, pages 11953–11962, 2022. [1](#), [3](#)
- [93] Hengshuang Zhao, Jianping Shi, Xiaojuan Qi, Xiaogang Wang, and Jiaya Jia. Pyramid scene parsing network. In *CVPR*, pages 2881–2890, 2017. [1](#), [2](#), [5](#), [6](#), [7](#), [8](#)
- [94] Hengshuang Zhao, Xiaojuan Qi, Xiaoyong Shen, Jianping Shi, and Jiaya Jia. Icnets for real-time semantic segmentation on high-resolution images. In *ECCV*, pages 405–420, 2018. [6](#)
- [95] Shuai Zheng, Sadeep Jayasumana, Bernardino Romera-Paredes, Vibhav Vineet, Zhizhong Su, Dalong Du, Chang Huang, and Philip HS Torr. Conditional random fields as recurrent neural networks. In *ICCV*, pages 1529–1537, 2015. [5](#)
- [96] Sixiao Zheng, Jiachen Lu, Hengshuang Zhao, Xiatian Zhu, Zekun Luo, Yabiao Wang, Yanwei Fu, Jianfeng Feng, Tao Xiang, Philip HS Torr, et al. Rethinking semantic segmentation from a sequence-to-sequence perspective with transformers. In *CVPR*, pages 6881–6890, 2021. [2](#), [3](#)
- [97] Xu Zheng, Yunhao Luo, Pengyuan Zhou, and Lin Wang. Distilling efficient vision transformers from cnns for semantic segmentation. *arXiv*, 2023. [3](#), [5](#), [8](#)
- [98] Zhaohui Zheng, Rongguang Ye, Ping Wang, Dongwei Ren, Wangmeng Zuo, Qibin Hou, and Ming-Ming Cheng. Localization distillation for dense object detection. In *CVPR*, 2022. [3](#)
- [99] Du Zhixing, Rui Zhang, Ming Chang, Shaoli Liu, Tianshi Chen, Yunji Chen, et al. Distilling object detectors with feature richness. In *NeurIPS*, pages 5213–5224, 2021. [3](#)
- [100] Bolei Zhou, Hang Zhao, Xavier Puig, Sanja Fidler, Adela Barriuso, and Antonio Torralba. Scene parsing through ade20k dataset. In *CVPR*, pages 633–641, 2017. [2](#), [5](#), [6](#), [7](#)
- [101] Yichen Zhu and Yi Wang. Student customized knowledge distillation: Bridging the gap between student and teacher. In *ICCV*, pages 5057–5066, 2021. [8](#)